Analytic density-functional self-consistent-field theory of diblock copolymers near patterned surfaces

Chaok Seok
Department of Pharmaceutical Chemistry, University of California in San Francisco, San Francisco, California 94143-2240

Karl F. Freed
James Franck Institute and Department of Chemistry, University of Chicago, Chicago, Illinois 60637

Igal Szleifer
James Franck Institute and Department of Chemistry, University of Chicago, Chicago, Illinois 60637 and Department of Chemistry, Purdue University, West Lafayette, Indiana 47907

(Received 15 December 2003; accepted 20 January 2004)

Analytical solutions are derived for the density profiles and the free energies of compressible diblock copolymer melts (or incompressible copolymer solutions) near patterned surfaces. The density-functional self-consistent-field theory is employed along with a Gaussian chain model for bonding constraints and a random mixing approximation for nonbonded interactions. An analytical solution is rendered possible by expanding the chain distribution function around an inhomogeneous reference state with a nontrivial analytical solution, by retaining the linear terms, and by requiring consistency with the homopolymer limit. The density profiles are determined by both real and complex roots of a sixth-degree polynomial that may easily be obtained by solving a generalized eigenvalue problem. This analytical formulation enables one to efficiently explore the large nine-dimensional parameter space and can serve as a first approximation to computationally intensive studies with more detailed models. Illustrative computations are provided for uniform and patterned surfaces above the order–disorder transition. The results are consistent with the previous self-consistent-field calculations in that lamellar ordering appears near the surface above the order–disorder transition and the lamella order perpendicular or parallel to the surface depending on the commensurability between the periods of the surface pattern and the density oscillations. © *2004 American Institute of Physics.* [DOI: 10.1063/1.1669372]

I. INTRODUCTION

The phenomenon of copolymer adsorption on chemically heterogeneous surfaces is technologically important, with numerous practical applications such as to lithography, lubrication, adhesion, etc.[1] Various theoretical, computational, and experimental studies have been performed for polymers at chemically patterned surfaces.[2,3] A major factor that controls the morphology of diblock copolymers has been found to be the commensurability between the two length scales: the period of the surface pattern and the natural period of polymer density oscillations. Relative strengths of the surface–polymer and polymer–polymer interactions also play a role.

This paper is the third of a series on applications of an analytical density-functional self-consistent-field formulation to polymer systems near chemically patterned walls. Analytical expressions for density profiles near patterned planar surfaces have previously been derived for polymer melts and incompressible solutions[4] and for polymer blends.[5] Here we extend the theory to present analytical solutions for diblock copolymer melts near patterned surfaces. (The theory also applies to the mathematically equivalent system of an incompressible copolymer solution, but for convenience, the discussion refers to a compressible polymer melt.) A simple Gaussian chain model and a random mixing approximation are used for analytical tractability, and a further first-order approximation is introduced for the influence of the surface to enable analytical resolution of the theory.

Within our analytical approximations, the density profiles near uniform walls are expressed as exponential or oscillating sine functions,[6,7] and those near patterned surfaces involve a Fourier series of the surface pattern.[4,5] The density profile for a homopolymer melt proximate to the uniform impenetrable surface emerges as an exponential function.[4,6] Those for a homopolymer blend are determined by the two roots of a quadratic equation[5,7] whose coefficients are nonlinear functions of the interaction and characteristic size parameters of the system. The blend density profiles are either decaying from the wall or oscillating throughout space, depending on whether the roots are real or complex and on whether they are positive or negative. The present extension to diblock copolymer melts near uniform or patterned surfaces finds that the density profiles depend on the roots of a sixth-degree polynomial when the theory is constrained to be consistent with the homopolymer limit. Exponential or oscillatory behaviors can appear depending on the phases of the roots of the polynomial. The same approach can easily be generalized to more complicated copolymer systems, such as

multiblock copolymers or copolymer mixtures, albeit resulting in higher-degree polynomials.

The number of characteristic parameters for even our minimal description of the system grows as the number of components and types of interactions increases. For diblock copolymers near a ''two-colored'' surface, there are nine relevant parameters: three monomer–monomer interactions, two monomer–wall interactions, two radii of gyration, and two bulk densities. A search for desired properties in the continuous parameter space of such a high dimension would be very costly, and our analytical formulation is well suited for such a purpose. More detailed models could be studied beginning from the approximate results obtained from our analytical theory.

Section II describes the extension of the analytical density-functional self-consistent-field formulation to diblock copolymer melts, and the monomer density profiles near uniform and patterned walls are derived in terms of the roots of a sixth-degree polynomial. Section III presents illustrative computations for systems above the bulk order–disorder transition, and the influence of the surfaces in modulating the surface densities is discussed.

II. THEORY

A. Density-functional self-consistent-field formulation of diblock copolymers

We consider a compressible diblock copolymer melt (or the mathematically equivalent incompressible copolymer solution) in the presence of an external field, where each molecule consists of two covalently bonded chains of type A and B, with polymerization indices N_A and N_B, respectively. The grand partition function Ξ for this system is

$$\Xi=\sum_{n=0}^{\infty}\frac{1}{n!}\int\cdots\int\Pi_{\alpha=1}^{n}\Pi_{i=1}^{N}d\mathbf{r}_{\alpha i}\exp\Bigg[-\beta V_n(\{\mathbf{r}_{\alpha i}\})+\sum_{\alpha}\left\{\sum_{i=1}^{N_A}w_A(\mathbf{r}_{\alpha i})+\sum_{i=N_A+1}^{N}w_B(\mathbf{r}_{\alpha i})\right\}\Bigg], \tag{1}$$

where β is $1/k_BT$, k_B is Boltzmann's constant, $N=N_A+N_B$, and $V_n(\{\mathbf{r}_{\alpha i}\})$ is the potential energy of a system of n diblock polymer molecules at configuration $\{\mathbf{r}_{\alpha i}\}$, where $\mathbf{r}_{\alpha i}$ denotes the position vector of the ith monomer in the αth molecule. $w_\lambda(\mathbf{r}_{\alpha i})$ ($\lambda=A$ or B) is the sum of the external potential (V_λ) and a term involving the chemical potential (μ_λ), $w_\lambda(\mathbf{r}_{\alpha i})=\beta\mu_\lambda/N_\lambda-\beta V_\lambda(\mathbf{r}_{\alpha i})$. The factors generated by the momentum integrals are omitted for simplicity. A Gaussian chain model is employed for the potential energy:

$$\beta V_n(\{\mathbf{r}_{\alpha i}\})=\sum_{\alpha=1}^{n}\sum_{i=1}^{N-1}\frac{3}{2l_i^2}|\mathbf{r}_{\alpha i+1}-\mathbf{r}_{\alpha i}|^2+\frac{1}{2}\sum_{(\alpha i)\neq(\alpha' i')}v_{ii'}(\mathbf{r}_{\alpha i}-\mathbf{r}_{\alpha' i'}), \tag{2}$$

where l_i is the Kuhn length and $v_{ii'}(\mathbf{r}_{\alpha i}-\mathbf{r}_{\alpha' i'})$ is the interaction potential between monomers.

The grand potential $\Omega=-kT\ln\Xi$ is a natural functional of $w_A(\mathbf{r})$ and $w_B(\mathbf{r})$ [Eq. (1)], and the functional derivative of $\beta\Omega$ with respect to $w_\lambda(\mathbf{r})$ ($\lambda=A$ or B) is equal to the average monomer density $\rho_\lambda(\mathbf{r})$:

$$\rho_\lambda(\mathbf{r})=-\frac{\delta(\beta\Omega)}{\delta w_\lambda(\mathbf{r})}, \tag{3}$$

where $\rho_A(\mathbf{r})=\langle\Sigma_\alpha\Sigma_{i=1}^{N_A}\delta(\mathbf{r}-\mathbf{r}_{\alpha i})\rangle$ and $\rho_B(\mathbf{r})=\langle\Sigma_\alpha\Sigma_{i=N_A+1}^{N}\delta(\mathbf{r}-\mathbf{r}_{\alpha i})\rangle$.

The Helmholtz free energy F is the Legendre transform of Ω,

$$F=\Omega+kT\sum_{\lambda=A,B}\int d\mathbf{r}\,\rho_\lambda(\mathbf{r})w_\lambda(\mathbf{r}), \tag{4}$$

and is a natural functional of $\rho_\lambda(\mathbf{r})$. The functional derivative of βF with respect to $\rho_\lambda(\mathbf{r})$ is

$$\frac{\delta(\beta F)}{\delta\rho_\lambda(\mathbf{r})}=w_\lambda(\mathbf{r}). \tag{5}$$

In the context of the density-functional theory, an ''ideal'' system is considered which has no nonbonded interactions between monomers, but has the same monomer density $\rho_\lambda(\mathbf{r})$ as the real system due to an artificial external potential $(kT)W_\lambda$, which is determined below. The grand potential of the ideal system is[6]

$$\Omega_{\mathrm{id}}=-kT\int d\mathbf{r}_1d\mathbf{r}_2d\mathbf{r}_3G_A(\mathbf{r}_1\mathbf{r}_2;0N_A)G_B(\mathbf{r}_2\mathbf{r}_3;N_AN), \tag{6}$$

where the end-vector distribution function G_λ is expressed in a path integral representation in the limit of continuous chains[8] as

$$G_\lambda(\mathbf{r}\mathbf{r}';NN')=\int_{\mathbf{r}(N)=\mathbf{r}}^{\mathbf{r}(N')=\mathbf{r}'}\mathcal{D}[\mathbf{r}(\tau)]\exp\Bigg[-\int_N^{N'}\frac{3}{2l_\lambda^2}\left|\frac{d\mathbf{r}(\tau)}{d\tau}\right|^2+\int_N^{N'}W_\lambda[\mathbf{r}(\tau)]\Bigg], \tag{7}$$

where W_λ is defined below.

The monomer density may be expressed in terms of the distribution function as

$$\rho_A(\mathbf{r})=\int d\mathbf{r}_1d\mathbf{r}_2d\mathbf{r}_3\int_0^{N_A}d\tau\,G_A(\mathbf{r}_1\mathbf{r};0\tau)\times G_A(\mathbf{r}\mathbf{r}_2;\tau N_A)G_B(\mathbf{r}_2\mathbf{r}_3;N_AN), \tag{8}$$

$$\rho_B(\mathbf{r})=\int d\mathbf{r}_1d\mathbf{r}_2d\mathbf{r}_3\int_{N_A}^{N}d\tau\,G_A(\mathbf{r}_1\mathbf{r}_2;0N_A)\times G_B(\mathbf{r}_2\mathbf{r};N_A\tau)G_B(\mathbf{r}\mathbf{r}_3;\tau N), \tag{9}$$

where the relation

$$\frac{\delta G_\lambda(\mathbf{r}'\mathbf{r}'';\tau'\tau'')}{\delta W_\lambda(\mathbf{r})}=\int_{\tau'}^{\tau''}d\tau\,G_\lambda(\mathbf{r}'\mathbf{r};\tau'\tau)G_\lambda(\mathbf{r}\mathbf{r}'';\tau\tau'') \tag{10}$$

is used.

As in the usual density-functional approaches, the Helmholtz free energy is written as

$$F = F_{\mathrm{id}} + F_{\mathrm{exc}}, \tag{11}$$

where $F_{\mathrm{id}} = \Omega_{\mathrm{id}} + kT\Sigma_\lambda \int d\mathbf{r}\, \rho_\lambda(\mathbf{r}) W_\lambda(\mathbf{r})$, thereby defining the excess free energy F_{exc}. The effective external potential $W_\lambda(\mathbf{r})$ follows upon using Eqs. (5), (10), and (11) as

$$W_\lambda(\mathbf{r}) = w_\lambda(\mathbf{r}) - \frac{\delta(\beta F_{\mathrm{exc}})}{\delta \rho_\lambda(\mathbf{r})}. \tag{12}$$

Following Ref. 6, a simple random mixing model of excluded volume interactions is used for the excess free energy, giving

$$\beta F_{\mathrm{exc}} = \frac{1}{2} \sum_{\lambda,\lambda'=A,B} v_{\lambda\lambda'} \int d\mathbf{r}\, \rho_\lambda(\mathbf{r}) \rho_{\lambda'}(\mathbf{r}). \tag{13}$$

The effective external potential with this excess free energy is

$$W_\lambda(\mathbf{r}) = \beta\mu_\lambda / N_\lambda - \beta V_\lambda(\mathbf{r}) - \sum_{\lambda'=A,B} v_{\lambda\lambda'} \rho_{\lambda'}(\mathbf{r}). \tag{14}$$

Within a linear approximation that relates $\rho_\lambda(\mathbf{r})$ and $W_\lambda(\mathbf{r})$, Eqs. (8), (9), and (14) can be solved analytically, as is described below.

B. Diblock copolymer melt near a uniform hard wall

Let us first consider a diblock copolymer melt near a uniform impenetrable hard wall. Bulk order–disorder transitions can also be obtained here because our approximation retains the linear response to the external field.[5] The extension to a patterned wall is considered in the next section.

A homogeneous melt in contact with a neutral hard wall at $z=0$ is taken as the reference state. The monomer density vanishes in the reference state for $z<0$ and is the same as the bulk density $\rho_{b\lambda}$ for $z \geqslant 0$. We then decompose $W_\lambda(z)$ into the reference term $W_\lambda^{(0)}(z)$ and the perturbation term $W_\lambda^{(1)}(z)$:

$$\begin{aligned} W_\lambda^{(0)}(z) &= \beta\mu_\lambda / N_\lambda - \beta V_\lambda^{(0)}(z) - \sum_{\lambda'=A,B} v_{\lambda\lambda'} \rho_{b\lambda'}, \\ W_\lambda^{(1)}(z) &= W_\lambda(z) - W_\lambda^{(0)}(z) \\ &= -\beta V_\lambda^{(1)}(z) - \sum_{\lambda'=A,B} v_{\lambda\lambda'} \delta\rho_{\lambda'}(z), \end{aligned} \tag{15}$$

where $\delta\rho_\lambda(z) = \rho_\lambda(z) - \rho_{b\lambda}$, $V_\lambda^{(0)}(z)$ is the neutral hard wall potential and the surface potential $V_\lambda^{(1)}(z) = V_\lambda(z) - V_\lambda^{(0)}(z)$ is approximated as $c_\lambda \delta(z)$, assuming it to be of short range.

The densities $\rho_\lambda(\mathbf{r})$ are obtained by expanding $G_\lambda(\mathbf{r},\mathbf{r}';\tau,\tau')$ around $W_\lambda^{(0)}(z)$ in Eqs. (8) and (9) using

$$\begin{aligned} G_\lambda(\mathbf{r},\mathbf{r}';\tau,\tau') = G_\lambda^{(0)}(\mathbf{r},\mathbf{r}';\tau,\tau') + \int d\mathbf{r}'' \int_\tau^{\tau'} d\tau'' \\ \times [G_\lambda^{(0)}(\mathbf{r},\mathbf{r}'';\tau,\tau'') G_\lambda^{(0)}(\mathbf{r}'',\mathbf{r}';\tau'',\tau') \\ \times W_\lambda^{(1)}(\mathbf{r}'')] + \mathcal{O}([W_\lambda^{(1)}]^2), \end{aligned} \tag{16}$$

which is derived from Eq. (10). The end-distribution function $G_\lambda^{(0)}(\mathbf{r},\mathbf{r}';\tau,\tau')$ for the reference system defined by the reference external potential $W_\lambda^{(0)}(z)$ is shown to be[9]

$$\begin{aligned} G_\lambda^{(0)}(\mathbf{r},\mathbf{r}';\tau,\tau') = \exp\left[\left(\beta\mu_\lambda/N_\lambda - \sum_{\lambda'} v_{\lambda\lambda'}\rho_{b\lambda'}\right)(\tau'-\tau)\right] \\ \times [G_{0\lambda}(z'-z;\tau'-\tau) \\ + G_{0\lambda}(z'+z;\tau'-\tau)] G_{0\lambda}(x'-x;\tau'-\tau) \\ \times G_{0\lambda}(y'-y;\tau'-\tau), \end{aligned} \tag{17}$$

where $G_{0\lambda}(z;\tau) = (3/2\pi\tau l_\lambda^2)^{1/2} \exp[-3z^2/2\tau l_\lambda^2]$.

Substituting the expanded $G_\lambda(\mathbf{r},\mathbf{r}';\tau,\tau')$ in Eqs. (8) and (9) and keeping terms to first order in $W_\lambda^{(1)}(z)$ gives

$$\begin{aligned} \delta\rho_A(z) &= J \int_0^\infty dz'\, K_A(z,z') W_A^{(1)}(z') \\ &\quad + J \int_0^\infty dz'\, K_{AB}(z,z') W_B^{(1)}(z'), \\ \delta\rho_B(z) &= J \int_0^\infty dz'\, K_B(z,z') W_B^{(1)}(z') \\ &\quad + J \int_0^\infty dz'\, K_{AB}(z,z') W_A^{(1)}(z'), \end{aligned} \tag{18}$$

where

$$J = \exp\left[\sum_\lambda \beta\mu_\lambda - \sum_{\lambda,\lambda'} v_{\lambda,\lambda'} \rho_{b\lambda'} N_\lambda\right], \tag{19}$$

$$\begin{aligned} K_\lambda(z,z') = N_\lambda^2 \int_{-\infty}^\infty (dk/2\pi) \\ [e^{ik(z-z')} + e^{ik(z+z')}] D(k^2 R_{g\lambda}^2), \end{aligned} \tag{20}$$

where $D(x) = (2/x^2)[x - 1 + \exp(-x)]$ is the Debye scattering function and

$$\begin{aligned} K_{AB}(z,z') = N_A N_B \int_{-\infty}^\infty (dk/2\pi) \\ \times [e^{ik(z-z')} + e^{ik(z+z')}] D_2(k^2 R_{gA}^2, k^2 R_{gB}^2), \end{aligned} \tag{21}$$

where $D_2(x_1,x_2) = 1/(x_1 x_2)[1-\exp(-x_1)][1-\exp(-x_2)]$.

The above integral equations (18) and (15) are solved by introducing cosine Fourier transformations. The cosine Fourier transformation of the density $\delta\rho_\lambda(z)$ can be expressed as

$$\begin{aligned} \begin{pmatrix} M_{AA}(k^2) & M_{AB}(k^2) \\ M_{BA}(k^2) & M_{BB}(k^2) \end{pmatrix} \begin{pmatrix} \delta\hat{\rho}_A(k) \\ \delta\hat{\rho}_B(k) \end{pmatrix} \\ = -\begin{pmatrix} C_{AA}(k^2) & C_{AB}(k^2) \\ C_{BA}(k^2) & C_{BB}(k^2) \end{pmatrix} \begin{pmatrix} c_A \\ c_B \end{pmatrix}, \end{aligned} \tag{22}$$

where

$$M_{\lambda\lambda}(\kappa)=1+a_{\lambda\lambda}v_{\lambda\lambda}D(\kappa r_\lambda)+a_{\lambda\lambda'}v_{\lambda\lambda'}D_2(\kappa r_\lambda,\kappa r_{\lambda'}),$$

$$M_{\lambda\lambda'}(\kappa)=a_{\lambda\lambda}v_{\lambda\lambda'}D(\kappa r_\lambda)+a_{\lambda\lambda'}v_{\lambda'\lambda'}D_2(\kappa r_\lambda,\kappa r_{\lambda'}),$$

$$C_{\lambda\lambda}(\kappa)=2a_{\lambda\lambda}D(\kappa r_\lambda),$$

$$C_{\lambda\lambda'}(\kappa)=2a_{\lambda\lambda'}D_2(\kappa r_\lambda,\kappa r_{\lambda'}),$$

$(\lambda,\lambda')=(A,B)$ or (B,A), where $a_{AA}=JN_A^2$, $a_{BB}=JN_B^2$, $a_{AB}=a_{BA}=JN_AN_B$, $r_A=R_{gA}^2$, $r_B=R_{gB}^2$, and $\kappa=k^2$.

To simplify the inverse Fourier transform, we use the common approximation $D(\kappa r_\lambda)\approx 2/(2+\kappa r_\lambda)$. A similar approximation for $D_2(\kappa r_A,\kappa r_B)$ is obtained by requiring that the correct limit of homopolymer melt be recovered when chemical identities of A and B monomers become the same, which implies

$$D_2(\kappa r_A,\kappa r_B)\approx\frac{1}{f_Af_B}\left[\frac{1}{2+\kappa r_A+\kappa r_B}-\frac{f_A^2}{2+\kappa r_A}-\frac{f_B^2}{2+\kappa r_B}\right], \tag{23}$$

where $f_\lambda=N_\lambda/N$.

After applying the above approximations the Fourier transform of the density then reduces to

$$\begin{pmatrix}\delta\hat{\rho}_A(k)\\ \delta\hat{\rho}_B(k)\end{pmatrix}=-\frac{1}{\det[P(\kappa)]}\begin{pmatrix}D_{AA}(\kappa) & D_{AB}(\kappa)\\ D_{BA}(\kappa) & D_{BB}(\kappa)\end{pmatrix}\begin{pmatrix}c_A\\ c_B\end{pmatrix}, \tag{24}$$

where $\det[P(\kappa)]$ is a sixth-degree polynomial in $\kappa=k^2$ and $D_{\lambda\lambda'}(\kappa)$ are fifth-degree polynomials in κ. (See Appendix A for the coefficients of the polynomials.)

All the real and complex roots of $\det[P(\kappa)]=0$ can be found numerically by solving a generalized eigenvalue problem (Appendix B). The above equation for $\delta\hat{\rho}_\lambda(k)$ can then be expressed in terms of the six roots $\kappa_0^\lambda,\kappa_1^\lambda,\ldots,\kappa_5^\lambda$ as

$$\begin{aligned}\delta\hat{\rho}_\lambda(k)&=-\frac{D_{\lambda\lambda}(\kappa)c_\lambda+D_{\lambda\lambda'}(\kappa)c_{\lambda'}}{\det[P(\kappa)]}\\&=\frac{d_0^\lambda+d_1^\lambda\kappa+\cdots+d_5^\lambda\kappa^5}{(\kappa-\kappa_0^\lambda)(\kappa-\kappa_1^\lambda)\cdots(\kappa-\kappa_5^\lambda)}\\&=\sum_i^r\frac{A_i^\lambda}{\kappa-\kappa_i^\lambda}+\sum_j^c\frac{B_{2j-1}^\lambda+B_{2j}^\lambda\kappa}{(\kappa-\kappa_j^\lambda)(\kappa-\kappa_j^{\lambda*})},\end{aligned} \tag{25}$$

where Σ_i^r is a summation over real roots κ_i^λ and Σ_j^c is a summation over complex conjugate root pairs κ_j^λ and $\kappa_j^{\lambda*}$. Here A_i^λ, B_{2j-1}^λ, and B_{2j}^λ are obtained by matching the coefficients, which is an easily solvable linear problem.

The inverse Fourier transformation of Eq. (25) gives the density profile in terms of the roots as follows:

$$\begin{aligned}\delta\rho_\lambda(z)=&\sum_i^{r_-}\frac{A_i^\lambda\exp(-a_i^\lambda z)}{2a_i^\lambda}-\sum_i^{r_+}\frac{A_i^\lambda\sin(a_i^\lambda z)}{2a_i^\lambda}\\&+\sum_j^c\frac{\exp(-a_j^\lambda z)}{2\sqrt{|\kappa_j^\lambda|}\sin\theta_j^\lambda}\left[\frac{B_{2j-1}^\lambda}{|\kappa_j^\lambda|}\sin\left(b_j^\lambda z+\frac{\theta_j^\lambda}{2}\right)\right.\\&\left.-B_{2j}^\lambda\sin\left(b_j^\lambda z-\frac{\theta_j^\lambda}{2}\right)\right],\end{aligned} \tag{26}$$

where Σ_i^{r-} and Σ_i^{r+} are summations over negative and positive real roots, respectively, and $a_i^\lambda=\sqrt{|\kappa_i^\lambda|}$ for a real root κ_i^λ, while $\kappa_j^\lambda=-|\kappa_j^\lambda|e^{i\theta_j^\lambda}$ and $\{-\kappa_j^\lambda\}^{1/2}=a_j^\lambda+ib_j^\lambda$ for a complex root pair κ_j^λ and $\kappa_j^{\lambda*}$. The above equation shows that a negative real root contributes an exponentially decaying term to the density profile, a positive real root to oscillations throughout all space, and a complex conjugate root pair to a decaying oscillatory term.

The same matrix $P(\kappa)$ describes the bulk density fluctuations in the linear response regime.[5] The bulk order–disorder transition can then be located by finding regions at which positive real roots of $\det[P(\kappa)]=0$ appear. The temperature at which positive real roots appear is the spinodal temperature, below which the ordered phase (oscillating density) becomes at least metastable. The thermodynamic transition temperature can be obtained by equating the free energies of the ordered and disordered phases. Once the equilibrium density profiles $\rho_\lambda(\mathbf{r})$ are obtained, the Helmholtz free energy can be obtained from the relation

$$\begin{aligned}F=&-\frac{kT}{2}\sum_{\lambda=A,B}\int d\mathbf{r}\frac{\rho_\lambda(\mathbf{r})}{N_\lambda}\\&+\frac{kT}{2}\sum_{\lambda,\lambda'=A,B}v_{\lambda\lambda'}\int d\mathbf{r}\,\rho_\lambda(\mathbf{r})\rho_{\lambda'}(\mathbf{r})\\&+kT\sum_{\lambda=A,B}\int d\mathbf{r}\,\rho_\lambda(\mathbf{r})W_\lambda(\mathbf{r}).\end{aligned} \tag{27}$$

Note that this equation satisfies relation (4). However, the functional $F[\{\rho_\lambda(\mathbf{r})\}]$ is not obtained in a closed form, but the free energy can be computed from the equilibrium densities using the above equation.

C. Diblock copolymer melt near a patterned wall

We now consider a hard wall potential with an arbitrary pattern that is specified by the spatially varying interaction parameters $c_\lambda(x,y)$ on the xy plane, $V_\lambda(\mathbf{r})=V_\lambda^{(0)}(z)+c_\lambda(x,y)\delta(z)$. The Fourier transform of the density is now expressed in terms of a three-dimensional vector $\mathbf{k}$ instead of k:

$$\begin{pmatrix}\delta\hat{\rho}_A(\mathbf{k})\\ \delta\hat{\rho}_B(\mathbf{k})\end{pmatrix}=-\frac{1}{\det[P(K)]}\begin{pmatrix}D_{AA}(K) & D_{AB}(K)\\ D_{BA}(K) & D_{BB}(K)\end{pmatrix}\times\begin{pmatrix}\hat{c}_A(\mathbf{k})\\ \hat{c}_B(\mathbf{k})\end{pmatrix}, \tag{28}$$

where $K=|\mathbf{k}|^2$. The Fourier representation of $c_\lambda(x,y)$ is written as

$$\begin{aligned}c_\lambda(x,y)&=\sum_{n,m=-\infty}^{\infty}c_{nm}^\lambda\exp[i(n_xx+m_yy)]\\&=\sum_{n,m=0}^{\infty}a_{nm}^\lambda\cos(n_xx+m_yy)\\&\quad+\sum_{n,m=1}^{\infty}b_{nm}^\lambda\sin(n_xx+m_yy),\end{aligned} \tag{29}$$

where $n_x = n\pi/L_x$, $m_y = m\pi/L_y$, L_x and L_y are length scales in the x and y directions of the surface pattern, and c^{λ}_{nm}, a^{λ}_{nm}, and b^{λ}_{nm} are the coefficients of the series.

Using the above series for the surface potential, the density profiles are also expressed in a Fourier series in the xy plane. This Fourier transform of the density profile is

$$\begin{aligned}
\delta\hat{\rho}_{\lambda}(\mathbf{k}) = &-\sum_{n,m=0}^{\infty} \frac{D_{\lambda\lambda}(K)a^{\lambda}_{nm} + D_{\lambda\lambda'}(K)a^{\lambda'}_{nm}}{\det[P(K)]}(2\pi)^2[\delta(\mathbf{k}_{xy}+\mathbf{n}_{xy}) + \delta(\mathbf{k}_{xy}-\mathbf{n}_{xy})] \\
&-\sum_{n,m=1}^{\infty} \frac{D_{\lambda\lambda}(K)b^{\lambda}_{nm} + D_{\lambda\lambda'}(K)b^{\lambda'}_{nm}}{\det[P(K)]}\frac{(2\pi)^2}{i}[\delta(\mathbf{k}_{xy}+\mathbf{n}_{xy}) - \delta(\mathbf{k}_{xy}-\mathbf{n}_{xy})] \\
&= \sum_{n,m=0}^{\infty}\left[\sum_{i}^{r}\frac{A^{c\lambda}_{nm,i}}{\mathbf{k}^2-K^{\lambda}_i} + \sum_{j}^{c}\frac{B^{c\lambda}_{nm,2j-1}+B^{c\lambda}_{nm,2j}\mathbf{k}^2}{(\mathbf{k}^2-K^{\lambda}_j)(\mathbf{k}^2-K^{\lambda}_j{}^*)}\right](2\pi)^2[\delta(\mathbf{k}_{xy}+\mathbf{n}_{xy}) + \delta(\mathbf{k}_{xy}-\mathbf{n}_{xy})] \\
&+ \sum_{n,m=1}^{\infty}\left[\sum_{i}^{r}\frac{A^{s\lambda}_{nm,i}}{\mathbf{k}^2-K^{\lambda}_i} + \sum_{j}^{c}\frac{B^{s\lambda}_{nm,2j-1}+B^{s\lambda}_{nm,2j}\mathbf{k}^2}{(\mathbf{k}^2-K^{\lambda}_j)(\mathbf{k}^2-K^{\lambda}_j{}^*)}\right]\frac{(2\pi)^2}{i}[\delta(\mathbf{k}_{xy}+\mathbf{n}_{xy}) - \delta(\mathbf{k}_{xy}-\mathbf{n}_{xy})], \qquad (30)
\end{aligned}$$

where $\mathbf{k}_{xy} = (\mathbf{k}\cdot\hat{x}, \mathbf{k}\cdot\hat{y})$, $\mathbf{n}_{xy} = (n_x, m_y)$, K^{λ}_i are the roots of $\det[P(K)]=0$, and $A^{c\lambda}_{nm,i}$, $B^{c\lambda}_{nm,2j-1}$, and $B^{c\lambda}_{nm,2j}$ are determined by the coefficients in the cosine series, while $A^{s\lambda}_{nm,i}$, $B^{s\lambda}_{nm,2j-1}$, and $B^{s\lambda}_{nm,2j}$ are determined by the sine series.

The three-dimensional inverse Fourier transformation gives the density profile as

$$\begin{aligned}
\delta\rho_{\lambda}(\mathbf{r}) = &\sum_{i}^{r_-}\sum_{n,m=0}^{\infty}\alpha^{\lambda}_{nm,i}(x,y)\frac{\exp(-a^{\lambda}_{nm,i}z)}{2a^{\lambda}_{nm,i}} + \sum_{i}^{r_+}\sum_{n,m=0}^{\infty}\alpha^{\lambda}_{nm,i}(x,y)\left[\frac{\exp(-a^{\lambda(-)}_{nm,i}z)}{2a^{\lambda(-)}_{nm,i}}H(\{a^{\lambda(-)}_{nm,i}\}^2)\right. \\
&\left. - \frac{\sin(a^{\lambda(+)}_{nm,i}z)}{2a^{\lambda(+)}_{nm,i}}H(\{a^{\lambda(+)}_{nm,i}\}^2)\right] + \sum_{j}^{c}\sum_{n,m=0}^{\infty}\frac{\exp(-a^{\lambda}_{nm,j}z)}{2|K^{\lambda}_j|\sin\theta^{\lambda}_j/\sqrt{|K^{\lambda}_{nm,j}|}}\left[\frac{\beta^{\lambda}_{nm,2j-1}(x,y)}{|K^{\lambda}_{nm,j}|}\sin\left(b^{\lambda}_{nm,j}z + \frac{\theta^{\lambda}_{nm,j}}{2}\right)\right. \\
&\left. - \beta^{\lambda}_{nm,2j}\sin\left(b^{\lambda}_{nm,j}z - \frac{\theta^{\lambda}_{nm,j}}{2}\right)\right], \qquad (31)
\end{aligned}$$

where

$$a^{\lambda}_{nm,i} = \sqrt{|K^{\lambda}_i| + n_x^2 + m_y^2},$$

$$\alpha^{\lambda}_{nm,i}(x,y) = A^{c\lambda}_{nm,i}\cos(n_x x + m_y y) + A^{s\lambda}_{nm,i}\sin(n_x x + m_y y),$$

$$a^{\lambda(-)}_{nm,i} = \sqrt{n_x^2 + m_y^2 - K^{\lambda}_i},$$

$$a^{\lambda(+)}_{nm,i} = \sqrt{K^{\lambda}_i - n_x^2 - m_y^2},$$

for a real root K^{λ}_i, where $H(x)=1$ if $x>0$ and 0 if $x<0$, and

$$|K^{\lambda}_j|e^{i\theta^{\lambda}_j} = -K^{\lambda}_j,$$

$$|K^{\lambda}_{nm,j}|e^{i\theta^{\lambda}_{nm,j}} = -K^{\lambda}_j + n_x^2 + m_y^2,$$

$$a^{\lambda}_{nm,j} + ib^{\lambda}_{nm,j} = (-K^{\lambda}_j + n_x^2 + m_y^2)^{1/2},$$

$$\beta^{\lambda}_{nm,2j-1}(x,y) = \{B^{c\lambda}_{nm,2j-1} + B^{c\lambda}_{nm,2j}(n_x^2+m_y^2)\}\cos(n_x x + m_y y) + \{B^{s\lambda}_{nm,2j-1} + B^{s\lambda}_{nm,2j}(n_x^2+m_y^2)\}\sin(n_x x + m_y y),$$

$$\beta^{\lambda}_{nm,2j}(x,y) = B^{c\lambda}_{nm,2j}\cos(n_x x + m_y y) + B^{s\lambda}_{nm,2j}\sin(n_x x + m_y y),$$

for a complex root pair K^{λ}_j and $K^{\lambda}_j{}^*$.

III. ILLUSTRATIVE COMPUTATIONS AND RESULTS

A. Bulk order–disorder transition of a diblock copolymer melt

There are seven parameters governing the bulk density fluctuations and thus determining the bulk order–disorder transition: the radii of gyration $R_{gA} = \sqrt{N_A/6}l_A$ and $R_{gB} = \sqrt{N_B/6}l_B$, the average bulk densities $\rho_{bA} = JN_A$ and $\rho_{bB} = JN_B$, and the pair interaction potentials (multiplied by β) v_{AA}, v_{BB}, and v_{AB}.

We can reduce the number of parameters to 5 by employing the freedom to choose the unit of length and by

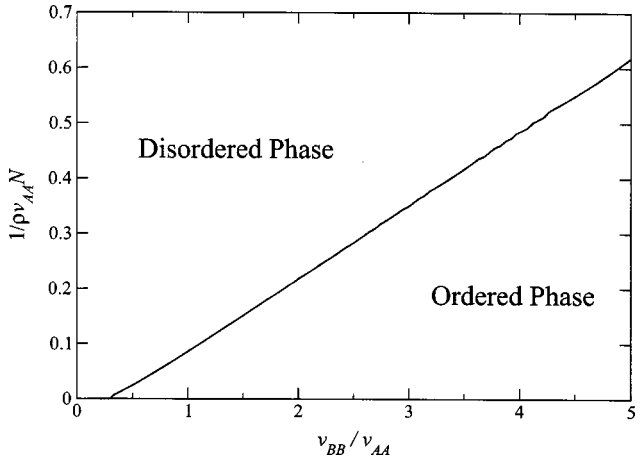

FIG. 1. Phase diagram showing the location of the ODT in parameter space. $N_A=N_B$, $R_{gB}=R_{gA}$, and $v_{AB}=2v_{BB}$. (The ordinate $1/\rho v_{AA}N$ is proportional to the temperature.)

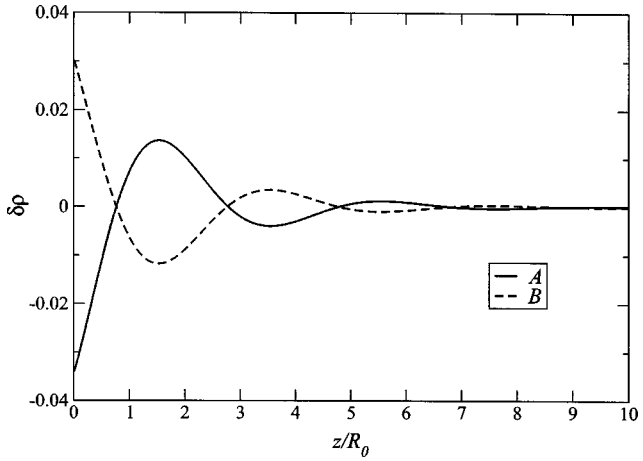

FIG. 2. Density profiles near a uniform hard wall above the ODT. Zero in the ordinate corresponds to the bulk density. Surface-induced density oscillations occur at this temperature ($1/\rho v_{AA}N=0.25$), which is higher than the transition temperature $1/\rho v_{AA}N=0.2173$. The oscillations indicate that the polymers order as lamella near the surface.

noting that the pair potentials $v_{\lambda\lambda'}$ always appear in an equation in the form $\rho v_{\lambda\lambda'}N$. Defining $R_0=\sqrt{N/6}l_A=R_{gA}\sqrt{N/N_A}$ as the unit of length, the five resulting parameters are $f_A=N_A/N$, $r_B^*=R_{gB}/R_{gA}$, $\rho v_{AA}N=JN^2v_{AA}$, $v_{BB}^*=v_{BB}/v_{AA}$, and $v_{AB}^*=v_{AB}/v_{AA}$. Note that J is defined in Eq. (19) and JN serves as the unit of density.

An illustrative phase diagram in the form of $\rho v_{AA}N$ versus v_{BB}/v_{AA} is presented in Fig. 1 and shows the parameter values at which a positive real root—and thus density oscillations—appears. The choice of $N_A=N_B$, $R_{gB}=R_{gA}$, and $v_{AB}=2v_{BB}$ is used to minimize the number of parameters. Using the Berthelot geometric average for $v_{AB}=\sqrt{v_{AA}v_{BB}}$ does not produce phase transitions in the range considered up to $v_{BB}/v_{AA}=100$. The line in Fig. 1 represents the spinodal curve, and the equilibrium transitions can be obtained by comparing the free energies of the ordered and disordered phases using Eq. (27).

B. Diblock copolymer melt near a uniform hard wall

The presence of a uniform hard wall introduces two additional surface potential parameters c_A and c_B beyond the five bulk parameters. These parameters are determined by specifying $\rho c_A N$ and $c_B^*=c_B/c_A$. Density profiles near the wall are depicted in Figs. 2–4 at varying temperatures and strengths of the surface interaction using the same parameters ($N_A=N_B$, $R_{gB}=R_{gA}$, and $v_{AB}=2v_{BB}$) as in Fig. 1, along with $v_{BB}/v_{AA}=2$. With this choice of parameters, the order of the strength of the monomer–monomer repulsion is $v_{AB}>v_{BB}>v_{AA}$. Figure 1 shows that the transition occurs at $1/\rho v_{AA}N=0.2173$ for this parameter choice. (Note that $1/\rho v_{AA}N$ is proportional to the temperature.)

Figures 2 and 3 exhibit the surface-induced density oscillations as appearing above the order–disorder transition temperature, with the amplitude of oscillations increasing as the transition temperature is approached. The temperatures chosen are $\rho v_{AA}N=0.25$ and 0.22, respectively, and the remaining parameters are $\rho c_A N=0.01\rho v_{AA}N$ and $c_B/c_A=-1$. The wall is attractive for B and repulsive for A. The choice of the wall–polymer interaction is consistent with the weak interaction assumption of the theory and provides an example in which one component (B) is preferentially favored over the other at the surface. Figure 4 displays the influence of different relative surface potentials $c_B/c_A=-2$ where the surface oscillations strengthen due to the greater surface adsorption of the B block.

C. Diblock copolymer melt near a patterned wall

The case of a striped wall with pattern length scale L_x is examined here as an example of a patterned surface. Application to more complicated wall potentials, such as one with a checkerboard pattern, is straightforward as in our previous works for homopolymers.[4]

Surface profiles above the order–disorder transition (ODT) are illustrated in Figs. 5, 6, and 7. The surface considered here has alternating stripes of surface potentials c_λ and $-c_\lambda$ of size L_x. Because the same parameters as in Fig.

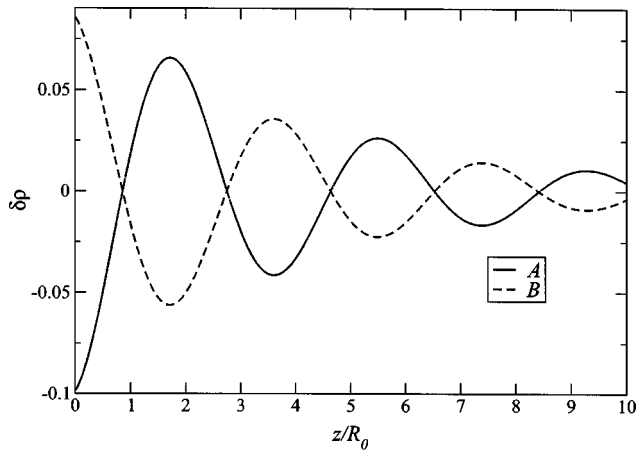

FIG. 3. Same as Fig. 2, except for $1/\rho v_{AA}N=0.22$, which is closer to the transition temperature. Surface lamellar ordering strengthens as the transition temperature is approached.

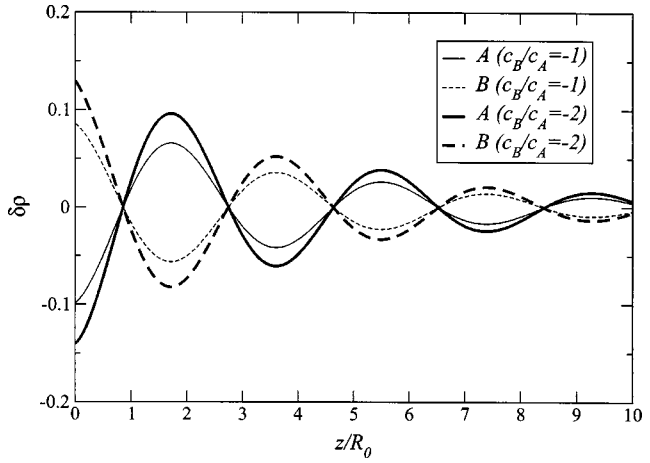

FIG. 4. Same as Fig. 3, except that the curves for $c_B/c_A=-2$ are shown together with the profiles in Fig. 2. Stronger attractive wall interactions for the *B* block strengthen the density oscillations.

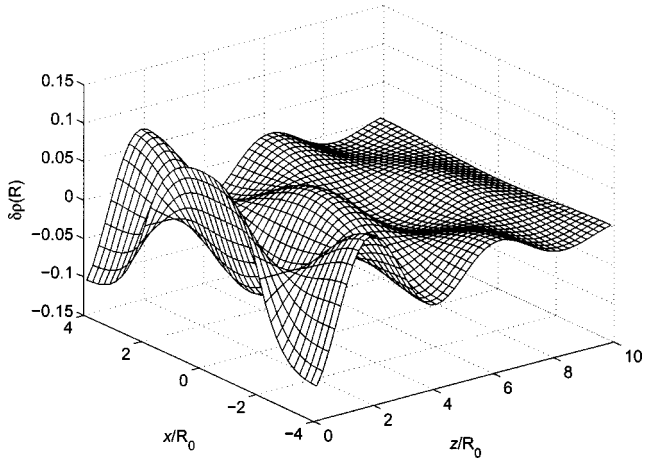

FIG. 6. Same as Fig. 5, except $L_x=4R_0$, which is twice as the surface oscillation length scale. For this large stripe size, the density oscillations in the *z* direction reappear as in Fig. 3 because the polymers order perpendicular to the surface.

3 are used, the stripes of one type are attractive for *A* and repulsive for *B*, and the opposite is true for the other type of stripes.

The orientation of the surface ordering depends on the relative sizes of the pattern period and the natural period of the density oscillations. Figure 5 considers the stripe width $L_x=1.9R_0$, which is the same as the half period of the surface oscillations in Fig. 3. In this commensurate case, density oscillations in the perpendicular direction that are present for the uniform surface become quenched, and the surface oscillations induced by the surface pattern dominate. This implies that the polymer does not order perpendicular to the surface, but orders parallel. Thus the lamella are perpendicular to the surface. The oscillations in the perpendicular direction reappear when the stripe size is increased, as displayed in Fig. 6 for $L_x=4R_0$. For a large surface pattern period, the polymers experience a locally homogeneous surface and, therefore, order perpendicular to the surface, resulting in a ''checkerboard'' morphology. This observation is consistent with the self-consistent-field calculation of Petera and Muthukumar.[3] When the pattern period is small compared to the lamellar period, the magnitude of the surface ordering diminishes significantly, as exhibited in Fig. 7. This implies that an appropriate surface pattern size might be used to tune the surface ODT from its bulk value. More studies of this behavior will be performed in the future.

IV. CONCLUSION

Analytical formulas have been derived for bulk density fluctuations and density profiles near planar uniform and patterned walls for diblock copolymer melts by extending our previous work for homopolymer melts and blends. Illustrative computations show that the analytical expressions produce consistent results with previous numerically more intensive works: density oscillations can be induced by the

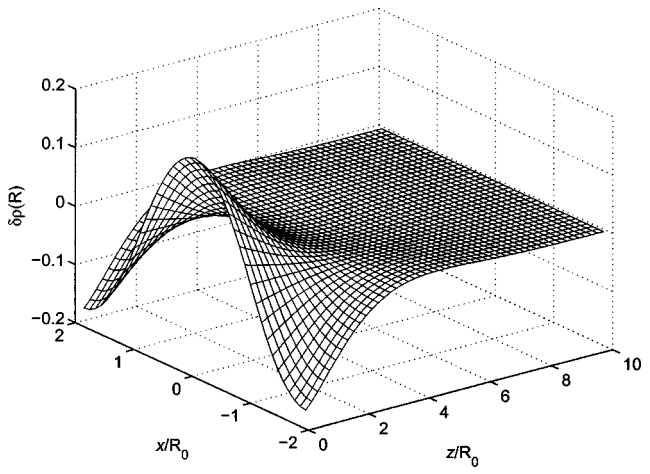

FIG. 5. Density profile of species *B* near a wall with striped pattern of width $L_x=1.9R_0$. The parameters are the same as in Fig. 3 for which lamellar ordering appears parallel to the uniform surface. The size of the stripes is the same as the half period of the surface oscillations of Fig. 3. In this commensurate case, the polymers order parallel to the surface, and the lamella are perpendicular to the surface. However, the density oscillations due to the lamellar ordering decay in the *z* direction because the stable bulk phase is disordered. Note that the *x* and *y* scales are different.

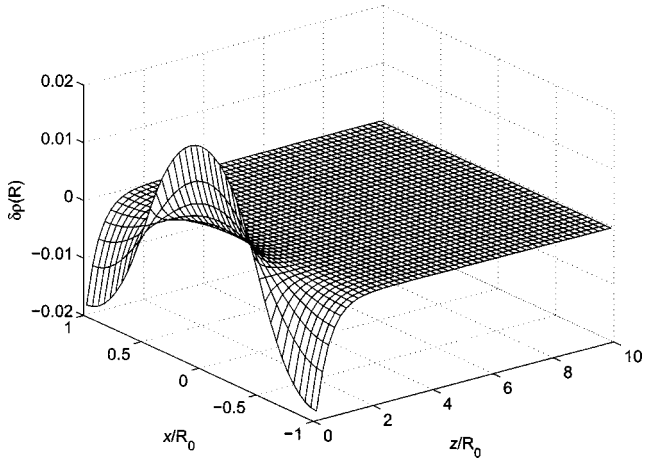

FIG. 7. Same as Fig. 5, except $L_x=R_0$, which is half of the size of the oscillation length scale. Density oscillations are much weaker than in Fig. 5 and are limited only in very close proximity to the wall for this small pattern size.

surface above the order–disorder transition temperature, and the orientation of the lamella depends on the commensurability of the pattern and lamella.

Our approach is limited to a Gaussian chain model and neglects chain deformation and orientation near the surface. In addition, the first-order approximation assumes weak polymer–surface interactions. More sophisticated models would no longer be analytically tractable and thus are computationally more expensive. The analytical solutions could be used as a starting point for numerical studies of more detailed models, and the agreement or deviation of the properties from the analytical results would provide insight into individual physical factors influencing the density profiles.

Surface behaviors below the order–disorder transition can in principle be treated in the same framework as presented in this paper and will be the subject of a future study. More complicated systems, such as thin films of copolymers confined between walls, are of considerable technological interest, and simulation studies for these situations are available.[10] Our theoretical approach could be extended to these cases. Analytical solutions, although complicated, are available for chain distribution functions for geometries other than planar, such as polymers confined within thin films or cylinders.[11] Those solutions could be utilized to extend the formalism to more complicated geometries.

APPENDIX A: COEFFICIENTS OF THE POLYNOMIALS

After multiplying

$$(2+\kappa r_A+\kappa r_B)(2+\kappa r_A)(2+\kappa r_B) \tag{A1}$$

on both sides of Eq. (22), we rewrite the equation as

$$P(\kappa)\begin{pmatrix}\delta\hat{\rho}_A(k)\\ \delta\hat{\rho}_B(k)\end{pmatrix}=-Q(\kappa)\begin{pmatrix}c_A\\ c_B\end{pmatrix}, \tag{A2}$$

where the components of the matrices $P(\kappa)$ and $Q(\kappa)$ are polynomials in κ as follows:

$$\begin{aligned}P_{\lambda\lambda}(\kappa)=&\,r_\lambda r_{\lambda'}(r_\lambda+r_{\lambda'})\kappa^3+[r_\lambda^2(2-a_{\lambda'\lambda'}v_{\lambda\lambda'})\\&+2r_\lambda r_{\lambda'}(3+a_{\lambda\lambda}v_{\lambda\lambda}+a_{\lambda\lambda'}v_{\lambda\lambda'})\\&+r_{\lambda'}^2\{2+a_{\lambda\lambda}(2v_{\lambda\lambda}-v_{\lambda\lambda'})\}]\kappa^2\\&+2[r_\lambda(4+2a_{\lambda\lambda}v_{\lambda\lambda}+2a_{\lambda\lambda'}v_{\lambda\lambda'}-a_{\lambda'\lambda'}v_{\lambda\lambda'})\\&+r_{\lambda'}\{4+a_{\lambda\lambda}(4v_{\lambda\lambda}-v_{\lambda\lambda'})+2a_{\lambda\lambda'}v_{\lambda\lambda'}\}]\kappa\\&+8(1+a_{\lambda\lambda}v_{\lambda\lambda}+a_{\lambda\lambda'}v_{\lambda\lambda'}),\end{aligned}$$

$$\begin{aligned}P_{\lambda\lambda'}(\kappa)=&[-r_\lambda^2a_{\lambda'\lambda'}v_{\lambda'\lambda'}+2r_\lambda r_{\lambda'}(a_{\lambda\lambda}v_{\lambda\lambda'}\\&+a_{\lambda\lambda'}v_{\lambda'\lambda'})+r_{\lambda'}^2a_{\lambda\lambda}(2v_{\lambda\lambda'}-v_{\lambda'\lambda'})]\kappa^2\\&+2[r_\lambda(2a_{\lambda\lambda}v_{\lambda\lambda'}-a_{\lambda'\lambda'}v_{\lambda'\lambda'}+2a_{\lambda\lambda'}v_{\lambda'\lambda'})\\&+r_{\lambda'}\{a_{\lambda\lambda}(4v_{\lambda\lambda'}-v_{\lambda'\lambda'})+2a_{\lambda\lambda'}v_{\lambda'\lambda'}\}]\kappa\\&+8(a_{\lambda\lambda}v_{\lambda\lambda'}+a_{\lambda\lambda'}v_{\lambda'\lambda'}),\end{aligned}$$

$$Q_{\lambda\lambda}(\kappa)=4a_{\lambda\lambda}[r_{\lambda'}(r_\lambda+r_{\lambda'})\kappa^2+2(r_\lambda+2r_{\lambda'})\kappa+4],$$

$$\begin{aligned}Q_{\lambda\lambda'}(\kappa)=&-2[a_{\lambda'\lambda'}r_\lambda^2-2a_{\lambda\lambda'}r_\lambda r_{\lambda'}+a_{\lambda\lambda}r_{\lambda'}^2]\kappa^2\\&+4[(2a_{\lambda\lambda'}-a_{\lambda'\lambda'})r_\lambda+(2a_{\lambda\lambda'}-a_{\lambda\lambda})r_{\lambda'}]\kappa\\&+16a_{\lambda\lambda'},\end{aligned}$$

where $(\lambda,\lambda')=(A,B)$ or (B,A).

The Fourier transform of the density is then

$$\begin{pmatrix}\delta\hat{\rho}_A(k)\\ \delta\hat{\rho}_B(k)\end{pmatrix}=-\frac{1}{\det[P(\kappa)]}\begin{pmatrix}D_{AA}(\kappa) & D_{AB}(\kappa)\\ D_{BA}(\kappa) & D_{BB}(\kappa)\end{pmatrix}\begin{pmatrix}c_A\\ c_B\end{pmatrix}, \tag{A3}$$

where

$$\begin{aligned}D_{AA}(\kappa)&=P_{BB}(\kappa)Q_{AA}(\kappa)-P_{AB}(\kappa)Q_{BA}(\kappa),\\D_{BB}(\kappa)&=-P_{BA}(\kappa)Q_{AB}(\kappa)+P_{AA}(\kappa)Q_{BB}(\kappa),\\D_{AB}(\kappa)&=P_{BB}(\kappa)Q_{AB}(\kappa)-P_{AB}(\kappa)Q_{BB}(\kappa),\\D_{BA}(\kappa)&=-P_{BA}(\kappa)Q_{AA}(\kappa)+P_{AA}(\kappa)Q_{BA}(\kappa).\end{aligned}$$

APPENDIX B: SOLVING THE POLYNOMIAL EQUATION

We solve the sixth-degree polynomial $\det[P(\kappa)]=0$ by converting it to a generalized eigenproblem following Manocha.[12]

The 2×2 matrix $P(\kappa)$ may be written as

$$P(\kappa)=P_0+P_1\kappa+P_2\kappa^2+P_3\kappa^3, \tag{B1}$$

where the P_i are 2×2 matrices independent of κ. Then the condition $\det[P(\kappa)]=0$ is equivalent to the generalized eigenvalue problem

$$\det(S_\kappa-H)=0, \tag{B2}$$

with

$$S=\begin{pmatrix}I & 0 & 0\\ 0 & I & 0\\ 0 & 0 & P_3\end{pmatrix} \tag{B3}$$

and

$$H=\begin{pmatrix}0 & I & 0\\ 0 & 0 & I\\ -P_0 & -P_1 & -P_2\end{pmatrix}, \tag{B4}$$

where I, 0, and P_i are 2×2 matrices, so S and H are 6×6 matrices. Therefore, the roots of $\det[P(\kappa)]=0$ are eigenvalues of the generalized eigenproblem

$$\kappa SV=HV, \tag{B5}$$

where V is the matrix of the right eigenvectors. This problem is solved using the lapack routine "dggev.f" (http://www.netlib.org/lapack/).

ACKNOWLEDGMENTS

This research is supported, in part, by NSF Grant No. CHE-0312226. I.S. acknowledges financial support from NSF Grant No. CTS-0001526.

[1] S. Walheim, E. Schaffer, J. Mlynek, and U. Steiner, Science **283**, 520 (1999); L. Gutman and A. K. Chakraborty, J. Chem. Phys. **101**, 10074 (1994); C. Harrison, M. Park, P. M. Chaikin, R. A. Register, D. H. Adamson, and N. Yao, Polymer **39**, 2733 (1998); M. Muthukumar, Curr. Opin. Colloid Interface Sci. **3**, 48 (1998); R. A. Segalman, H. Yokoyama, and E. J. Kramer, Adv. Mater. (Weinheim, Ger.) **13**, 1152 (2001); S. O. Kim, H. H. Solak, M. P. Stoykovich, N. J. Ferrier, J. J. de Pablo, and P. F. Nealey, Nature (London) **424**, 411 (2003).
[2] Y. Tsori and A. Andelman, Macromolecules **34**, 2719 (2001); Europhys. Lett. **53**, 722 (2001); D. Petera and M. Muthukumar, J. Chem. Phys. **109**, 5101 (1998); L. Kielhorn and M. Muthukumar, *ibid.* **111**, 2259 (1999); J. Genzer, *ibid.* **115**, 4873 (2001); A. C. Balazs, Acc. Chem. Res. **26**, 63 (1993); K. Binder, Physica A **200**, 722 (1993); K. Binder and M. Muller, Curr. Opin. Colloid Interface Sci. **5**, 315 (2000); P. G. Degennes, Macromolecules **13**, 1069 (1980); P. F. Green and T. P. Russell, *ibid.* **25**, 783 (1992); F. A. M. Leermakers and A. P. Gast, *ibid.* **24**, 718 (1991); M. R. Munch and A. P. Gast, J. Chem. Soc., Faraday Trans. **86**, 1341 (1990); O. A. Evers, J. Scheutjens, and G. J. Fleer, Macromolecules **23**, 5221 (1990); O. A. Evers, J. Scheutjens, and G. J. Fleer, *ibid.* **24**, 5558 (1991); K. Y. Chun, Y. W. Huang, and V. K. Gupta, J. Chem. Phys. **118**, 3252 (2003); G. J. Fleer and J. Scheutjens, Colloids Surf. **51**, 281 (1990); C. Park, J. Yoon, and E. L. Thomas, Polymer **44**, 6725 (2003); Q. Wang, P. F. Nealey, and J. J. de Pablo, Macromolecules **35**, 9563 (2002); J. J. Semier and J. Genzer, J. Chem. Phys. **119**, 5274 (2003).
[3] D. Petera and M. Muthukumar, J. Chem. Phys. **107**, 9640 (1997).
[4] C. Seok, K. F. Freed, and I. Szleifer, J. Chem. Phys. **112**, 6443 (2000).
[5] C. Seok, K. F. Freed, and I. Szleifer, J. Chem. Phys. **112**, 6452 (2000).
[6] K. F. Freed, J. Chem. Phys. **103**, 3230 (1995).
[7] K. F. Freed, J. Chem. Phys. **105**, 10 572 (1996).
[8] K. F. Freed, *Renormalization Group Theory of Macromolecules* (Wiley-Interscience, New York, 1987).
[9] A. M. Nemirovsky and K. F. Freed, J. Chem. Phys. **83**, 4166 (1985).
[10] Q. Wang, Q. L. Yan, P. F. Nealey, and J. J. de Pablo, J. Chem. Phys. **112**, 450 (2000); Q. Wang, S. K. Nath, M. D. Graham, P. F. Nealey, and J. J. de Pablo, *ibid.* **112**, 9996 (2000); Q. Wang, P. F. Nealey, and J. J. de Pablo, Macromolecules **34**, 3458 (2001); Q. Wang, Q. L. Yan, P. F. Nealey, and J. J. de Pablo, *ibid.* **33**, 4512 (2000).
[11] Z.-G. Wang, A. M. Nemirovsky, and K. F. Freed, J. Chem. Phys. **86**, 4266 (1987).
[12] D. Manocha, IEEE Comput. Graphics Appl. **14**, 46 (1994).